

# First-principles study on magnetic tunneling junctions with semiconducting $\text{CuInSe}_2$ and $\text{CuGaSe}_2$ barriers

Keisuke Masuda<sup>1</sup> and Yoshio Miura<sup>1,2,3,4</sup>

<sup>1)</sup>*Research Center for Magnetic and Spintronic Materials,  
National Institute for Materials Science (NIMS), 1-2-1 Sengen, Tsukuba 305-0047,  
Japan*

<sup>2)</sup>*Kyoto Institute of Technology, Electrical Engineering and Electronics,  
Kyoto 606-8585, Japan*

<sup>3)</sup>*Center for Materials Research by Information Integration,  
National Institute for Materials Science (NIMS), 1-2-1 Sengen, Tsukuba 305-0047,  
Japan*

<sup>4)</sup>*Center for Spintronics Research Network (CSRN), Graduate School of Engineering  
Science, Osaka University, Machikaneyama 1-3, Toyonaka, Osaka 560-8531,  
Japan*

(Dated: 28 September 2016)

We theoretically investigate two different magnetic tunneling junctions (MTJs) with semiconductor barriers,  $\text{CuInSe}_2$  (CIS) and  $\text{CuGaSe}_2$  (CGS), which are the terminal compounds of recently reported mixed semiconductor barrier,  $\text{CuIn}_{1-x}\text{Ga}_x\text{Se}_2$ . To discuss the transport properties of these systems, we analyze complex band structures, magnetoresistance (MR) ratios, and resistance-area products ( $RA$ ) by using first-principles based calculations in combination with the Landauer formula. It is found that the  $\Delta_1$  wave functions have dominant contributions to the spin-dependent tunneling transport in both CIS- and CGS-based MTJs. We also find that the CGS-based MTJ has a much larger MR ratio and slightly higher  $RA$  than those of the CIS-based MTJ, which indicates that a larger MR ratio is expected for a higher Ga concentration  $x$  in the  $\text{CuIn}_{1-x}\text{Ga}_x\text{Se}_2$ -based MTJs. We further study the relationship between the band gaps in the barriers and MR ratios by changing the Coulomb repulsions in the Cu  $3d$  states of the CIS and CGS. It is shown that the barrier with a larger band gap yields a larger MR ratio. The comparison of MR ratios and  $RA$  between the CIS-, CGS-, and MgO-based MTJs are also given.

Magnetoresistive (MR) devices with high MR ratios and low resistance-area products ( $RA$ ) are required for realizing read sensors of ultrahigh density hard disk drives and Gbit class spin transfer torque magnetoresistive random access memories (STT-MRAMs). Various attempts have been made to reduce  $RA$  of MgO-based MTJs<sup>1,2</sup> to less than  $1\ \Omega\ \mu\text{m}^2$  while keeping high tunneling magnetoresistance (TMR) ratios. Elaborate techniques to deposit ultrathin MgO barriers ( $\sim 1\text{nm}$ ) have been established,<sup>3-5</sup> which enabled the reduction of the  $RA$  to  $\sim 1\ \Omega\ \mu\text{m}^2$  keeping the high MR ratio of around 200 % at room temperature. On the other hand, the use of half-metallic Co-based Heusler alloys as ferromagnetic (FM) electrodes increased the value of the MR ratio in low- $RA$  current-perpendicular-to-plane giant magnetoresistive (CPP-GMR) devices.<sup>6-11</sup> The highest MR ratio reported so far is 82 % at room temperature for the  $\text{Co}_2\text{FeGa}_{0.5}\text{Ge}_{0.5}/\text{Ag}/\text{Co}_2\text{FeGa}_{0.5}\text{Ge}_{0.5}$  system with the  $RA$  value of  $\sim 40\ \text{m}\Omega\ \mu\text{m}^2$ .<sup>11</sup> However, this  $RA$  value is too low to obtain sufficiently high voltage output under current for read sensor applications. Most recently, Kasai *et al.* reported a high MR ratio of 40% at room temperature and 100% at 8 K in the MTJ using the compound semiconductor  $\text{CuIn}_{0.8}\text{Ga}_{0.2}\text{Se}_2$  (CIGS) with the chalcopyrite crystal structure as a barrier in combination with the  $\text{Co}_2\text{FeGa}_{0.5}\text{Ge}_{0.5}$  FM layers.<sup>12</sup> This is the first observation of high MR output for MTJs with a compound semiconductor barrier. Since the band gap of the CIGS is much smaller than that of the insulator MgO, a smaller  $RA$  is expected. Actually, sufficiently small  $RA$  values ranging from 0.3 to  $3\ \Omega\ \mu\text{m}^2$  were observed in the CIGS-based MTJs. Moreover, these MTJs are expected to have high controllability and high breakdown voltage because their barrier thicknesses ( $\sim 2\text{nm}$ ) are two times longer than those of the above-mentioned MgO-based MTJs with comparably low  $RA$ . Such semiconductor barriers open up another way to realize both low  $RA$  and high MR output.

From the theoretical point of view, several previous studies have focused on the transport properties of the MTJs with semiconductor barriers. MacLaren *et al.*<sup>13</sup> have studied the MTJs consisting of Fe electrodes and a semiconductor barrier ZnSe within the first-principles calculations using the layer Korringa-Kohn-Rostoker approach. They have shown that the system has spin-dependent tunneling transport properties, in which the  $\Delta_1$  bands have dominant contributions. From their data, the MR ratio was estimated to be  $\sim 500\%$  for the barrier of 50 a.u. ( $\sim 2.6\text{nm}$ ). Another theoretical work by Autès *et al.*<sup>14</sup> discussed the MTJ composed of a GaAs barrier sandwiched with Fe electrodes. They calculated spin-dependent conductance and predicted a maximum MR ratio of nearly 400 % for around 10

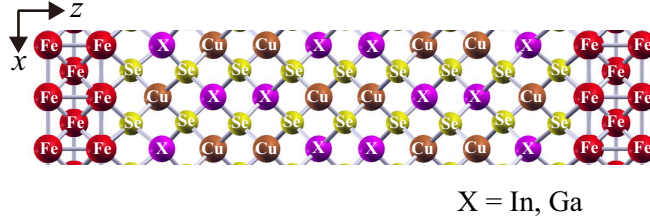


FIG. 1. Schematic picture of the supercell used in this study.

atomic layers of GaAs. Moreover, they took into account the spin-orbit interaction and found that the effect of the interaction is significant for sufficiently thick barriers ( $\gg 20$  atomic layers  $\sim 2.8$  nm). Although these theoretical approaches have predicted large MR ratios, such notable output has not been experimentally observed in the ZnSe- and GaAs-based MTJs; only a small MR ratio ( $< 2\%$ ) has been reported in the GaAs-based MTJs.<sup>15,16</sup> On the other hand, no theoretical studies have focused on the CIGS-based MTJs in spite of the recent report on large MR output. To understand the origin of such a large MR ratio in low- $RA$  TMR devices, theoretical understanding on the transport properties of FM/CIGS/FM MTJs is essential.

In this work, we study transport properties of two MTJs with different barriers,  $\text{CuInSe}_2$  (CIS) and  $\text{CuGaSe}_2$  (CGS), which are the terminal compounds of  $\text{CuIn}_{1-x}\text{Ga}_x\text{Se}_2$  mixed crystal. Since the band gap of  $\text{CuIn}_{1-x}\text{Ga}_x\text{Se}_2$  continuously increases as  $x$  increases, the CIGS is located between CIS and CGS not only chemically but also physically. Therefore, the present study for the CIS and CGS terminal compounds is sufficient to obtain enough information on the CIGS-based MTJ. As electrodes, we adopt ferromagnetic bcc Fe with well-known band structure. Since the  $a$ -axis length of the CIS (CGS) is almost twice as long as that of bcc Fe, the lattice mismatch between them is expected to be quite small. Note that we do not consider the effect of the spin-orbit interaction in this work, because we focus on thin barrier of  $\sim 2$  nm, in which the effect of the spin-orbit interaction is sufficiently small as shown in the related study on the MTJ with a GaAs barrier.<sup>14</sup>

We prepared the supercells of Fe/CIS/Fe and Fe/CGS/Fe (Fig. 1), each of which includes 2 unit cells (=17 layers) of CIS or CGS and 1 unit cell (=3 layers) of Fe in both sides of the barrier. This length of the barrier is comparable to 2 nm estimated in the experiments on the CIGS-based MTJ.<sup>12</sup> We fixed the  $a$ -axis length to 0.5782 nm in the case of CIS<sup>17</sup> and to 0.5614 nm in the case of CGS.<sup>18</sup> As termination layers, we selected Se layers, which is

also based on the TEM observation results in the experimental work.<sup>12</sup> We next optimized the positions of atoms in the supercells by using the density-functional theory within the generalized-gradient approximation which is implemented in the Vienna *ab-initio* simulation program (VASP).<sup>19,20</sup> In this optimization, we used  $10 \times 10 \times 1$   $\mathbf{k}$ -point mesh and assume that the spins of all Fe atoms align parallel each other. As the result of the calculation, the distance between Fe and Se layers in the CIS-based (CGS-based) supercell is determined as  $\sim 0.167$  nm ( $\sim 0.144$  nm) in the left boundary and as  $\sim 0.168$  nm ( $\sim 0.151$  nm) in the right boundary. Such a difference in the distance between the left and right boundaries is due to the lack of the inversion symmetry along the  $c$ -axis in the CIS and CGS.

To discuss the transport properties of the CIS- and CGS-based MTJs, we consider the quantum open system composed of the above-mentioned supercell attached to the left and right semi-infinite electrodes of Fe atoms. The conductance calculations were done with the aid of the quantum code ESPRESSO.<sup>21</sup> In the present work, the Coulomb repulsion  $U$  for the Cu  $3d$  states in the barriers was taken into account to investigate the change in the MR ratio by changing the amplitude of the band gap systematically.<sup>22,23</sup> First, we obtained the wave functions in each region of the quantum open system by means of the density-functional theory and the generalized-gradient approximation. The number of  $\mathbf{k}$  points was taken as  $10 \times 10 \times 1$ , and Methfessel-Paxton smearing with a broadening parameter 0.01 Ry was used. The cutoff energy for the wave function and charge density was set to 30 and 300 Ry, respectively. Since our system has a two-dimensional periodicity in the  $xy$  plane, the scattering states can be classified by an in-plane wave vector  $\mathbf{k}_{\parallel} = (k_x, k_y)$ . For each fixed  $\mathbf{k}_{\parallel}$  and spin index, we solved the scattering equations derived from the condition that the wave function and its derivative in the supercell are connected to those in the electrodes.<sup>24,25</sup> In this process, we can also obtain the complex band structures, which are useful to understand transport properties of the system. Conductance is calculated by substituting the amplitudes of the scattering wave functions into the Landauer formula.

We first fixed the Coulomb repulsion  $U$  to 5 eV and focused on the difference between the CIS- and CGS-based MTJs. Figures 2 (a) and 2 (b) show the real and complex band structures of the CIS and CGS, respectively, at  $\mathbf{k}_{\parallel} = (0, 0)$  along the out-of-plane wave vector  $k_z$ . The band gaps are estimated as  $E_g^{\text{CIS}} \simeq 0.17$  eV for the CIS and  $E_g^{\text{CGS}} \simeq 0.41$  eV for the CGS. Although these values are smaller than the experimental observations ( $E_g^{\text{CIS}} \simeq 1.0$  eV and  $E_g^{\text{CGS}} \simeq 1.7$  eV), magnitude relation ( $E_g^{\text{CIS}} < E_g^{\text{CGS}}$ ) is the same for the present

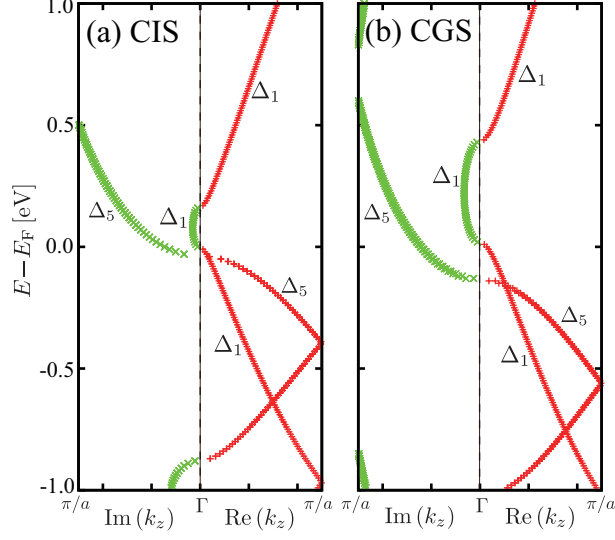


FIG. 2. Real and complex band structures of (a) CIS and (b) CGS with  $U = 5$  eV at  $\mathbf{k}_{\parallel} = (0, 0)$  along the out-of-plane wave vector  $k_z$ .

calculations and experiments. We see that the complex band with the  $\Delta_1$  components has the smallest imaginary part  $\kappa_{\min} = |\text{Im}(k_z)|_{\min}$  around the Fermi level in both CIS and CGS. This means that the propagating state with the  $\Delta_1$  components in the electrode couple to the evanescent state ( $\kappa_{\min}$ ) in the barrier and makes the largest contribution to the tunneling conductance.<sup>26</sup>

In Fig. 3, we show the in-plane wave vector  $\mathbf{k}_{\parallel} = (k_x, k_y)$  dependence of the conductances at the Fermi energy for various situations in the CIS- and CGS-based MTJs. The upper two panels, Figs. 3(a) and 3(d), show the majority-spin conductances of the CIS and CGS MTJs with parallel magnetization of the electrodes, in which the sharp peaks around  $\mathbf{k}_{\parallel} = (0, 0)$  are seen for both the MTJs. As shown in Figs. 2 (a) and 2 (b), since the  $\Delta_1$  evanescent state is the dominant conducting channel at  $\mathbf{k}_{\parallel} = (0, 0)$  in the barriers, these peaks can be considered as evidence for the tunneling transport by the  $\Delta_1$  wave functions. Figures 3(b) and 3(e) show the minority-spin conductances of the CIS- and CGS-based MTJs with parallel magnetization of the electrodes. Compared to the majority-spin cases, conductances have much smaller values and distribute over a wide region of the  $\mathbf{k}_{\parallel}$  Brillouin zone for both the CIS- and CGS-based MTJs. Note that in Fe electrodes, not only the majority-spin channel but also the minority-spin channel has the  $s$  band crossing the Fermi level in the  $(0, 0, k_z)$  direction due to the band folding.<sup>27</sup> However, the folded minority-spin band

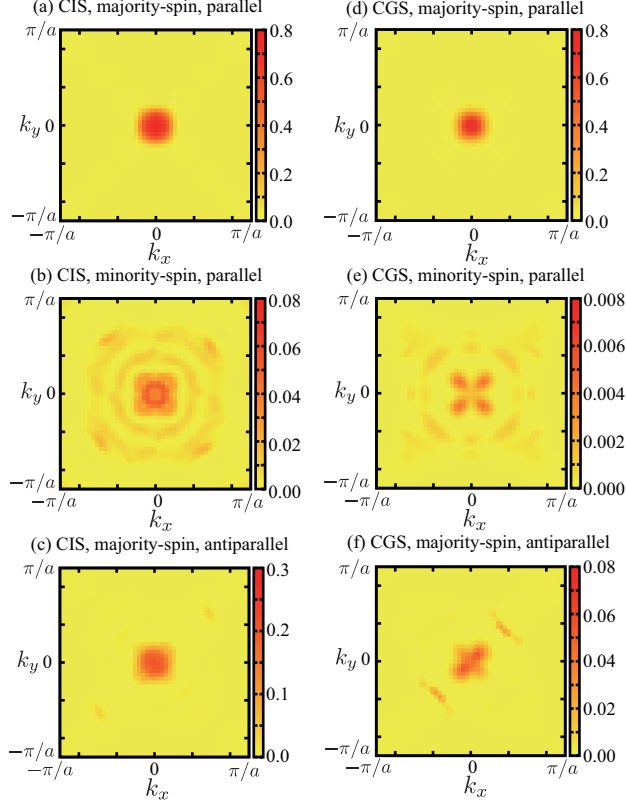


FIG. 3. In-plane wave vector  $\mathbf{k}_{\parallel} = (k_x, k_y)$  dependence of the conductances at the Fermi energy for various cases in the CIS- and CGS-based MTJs with  $U = 5\text{ eV}$ . (See the text in detail.) The unit of the color bar is  $G_0 = e^2/h$  in all the panels.

has no contribution to the conductance in both the CIS- and CGS-based MTJs, which is different from the case of the Fe/MgAl<sub>2</sub>O<sub>4</sub>(MAO)/Fe MTJ with not so small minority-spin conductance.<sup>27</sup> In the MAO-based MTJ, the oxygen atoms dominating the electron transport have four-fold rotational symmetry in the  $xy$  plane as the result of the structure relaxation.<sup>27</sup> On the other hand, the CIS and CGS have only two-fold rotational symmetry in the  $xy$  plane, which might be the reason for the different spin-dependent transport between the MAO-based and CIS(CGS)-based MTJs. The lower two panels, Figs. 3(c) and 3(f), show the conductances of the CIS- and CGS-based MTJs for the majority-spin states of the left electrodes in the case of the antiparallel magnetization. Although the  $\Delta_1$  wave function in the left electrode decays more rapidly than the parallel-magnetization case, it still has a small amplitude in the right electrode after passing through the barrier, which is the origin of the small conductances around  $\mathbf{k}_{\parallel} = (0, 0)$ . Note that the  $\mathbf{k}_{\parallel}$  dependences in Figs. 3(c) and 3(f) break four-fold rotational symmetry, which might be due to the two-fold symmetry

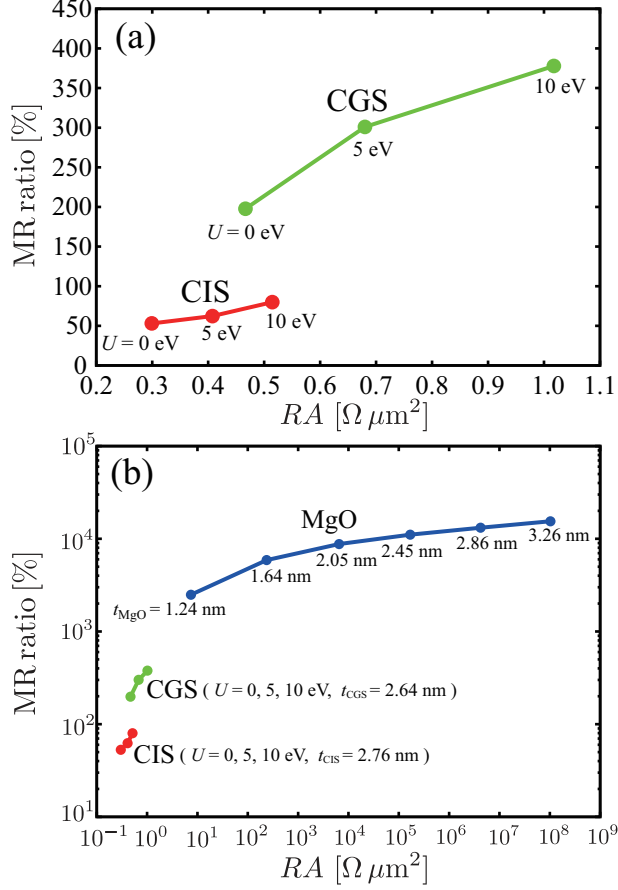


FIG. 4. Comparison of MR ratios and  $RA$  (a) between CIS- and CGS-based MTJs and (b) between CIS-, CGS-, and MgO-based MTJs on a double-logarithmic scale. In the panel (b), the barrier thickness ( $t_{\text{CIS}}$ ,  $t_{\text{CGS}}$ ,  $t_{\text{MgO}}$ ) is defined as a distance between two Fe layers closest to the barrier.

of the CIS and CGS in the  $xy$  plane. Although we do not show here, the minority-spin conductances in the case of the antiparallel magnetization have the  $\mathbf{k}_{\parallel}$  dependences that are identical with those obtained by rotating Figs. 3(c) and 3(f) by  $180^\circ$  in the  $\mathbf{k}_{\parallel}$  plane.

In this work, we adopt the usual optimistic definition of the MR ratio:  $\text{MR ratio} [\%] = 100 \times (T_{\text{P}} - T_{\text{AP}})/T_{\text{AP}}$ , where  $T_{\text{P}}$  ( $T_{\text{AP}}$ ) is the sum of the majority- and minority-spin conductances averaged over the  $\mathbf{k}_{\parallel}$  Brillouin zone in the case of the parallel (antiparallel) magnetization. We obtained 62.3 and 300.9% MR ratios for the CIS- and CGS-based MTJs, respectively. This difference is mainly due to a large difference in conductances in the case of the antiparallel magnetization (Figs. 3(c) and 3(f)). We also estimated  $RA$  values from the conductances in the case of the parallel magnetization  $T_{\text{P}}$ , where 0.408 and  $0.680 \Omega \mu\text{m}^2$  were obtained for the CIS- and CGS-based MTJs, respectively.

Let us further discuss the relationship between the band gaps and MR ratios by changing the Coulomb repulsion  $U$  for the Cu  $3d$  states in the barriers. By increasing the repulsion  $U$  from 0 to 10 eV, the band gap of bulk CIS (CGS) is increased from 0.044 (0.114) to 0.468 (0.691) eV. In Fig. 4(a), we show the MR ratios and  $RA$  for the CIS- and CGS-based MTJs with  $U = 0, 5$ , and 10 eV. As the repulsion  $U$  becomes larger, the MR ratio and  $RA$  become higher in both the MTJs. It is also found that for a fixed repulsion  $U$ , the CGS-based MTJ has a larger MR ratio and higher  $RA$  than those of the CIS-based MTJ. From these, we can conclude, at least for the CIS- and CGS-based MTJs, that a larger gap system has a larger MR ratio and higher  $RA$ .

Figure 4(b) shows the comparison of MR ratios and  $RA$  for the CIS-, CGS-, and MgO-based MTJs. The MR ratios and  $RA$  of the MgO-based MTJ are calculated in the same way as those of the CIS- and CGS-based MTJs. For the barrier thickness of  $2.6 \sim 2.8$  nm, the  $RA$  values for the CIS- and CGS-based MTJs are nearly six orders magnitude smaller than those for the MgO-based MTJs, which is a great advantage of the CIS- and CGS-based MTJs for certain device applications where low  $RA$  is needed, e.g., read sensors. Even if we reduce the thickness of the MgO to 1.24 nm,  $RA$  is still larger than those of the CIS and CGS systems. On the other hand, the CIS- and CGS-based MTJs have a possibility of achieving further low  $RA$  values by reducing their barrier thicknesses. In that case, establishing a method to keep the MR ratio high, e.g., the use of the highly spin-polarized ferromagnetic electrodes, would be essential. In fact, such an example was recently reported by Kasai *et al.*<sup>12</sup>

In summary, we have studied transport properties of the MTJs with semiconductor barriers, Fe/CIS/Fe and Fe/CGS/Fe. Our first-principles based calculations have shown that the  $\Delta_1$  wave functions dominate the tunneling transport in both the MTJs. The theoretical transport calculations have predicted the MR ratios of around 50 % for the CIS-based MTJ and around 300 % for the CGS-based one, which means that a larger MR ratio is expected for a higher Ga concentration  $x$  in the  $\text{CuIn}_{1-x}\text{Ga}_x\text{Se}_2$ -based MTJs. We have further discussed the relationship between the band gaps and MR ratios by changing the value of the Coulomb repulsion in the CIS and CGS barriers. We found that a larger band gap in the barrier gives a larger MR ratio. Through the comparison with MgO-based MTJ, we have confirmed that the CIS- and CGS-based MTJs have much smaller  $RA$  than the MgO-based one, which is consistent with the experimental results on the  $\text{CuIn}_{0.8}\text{Ga}_{0.2}\text{Se}_2$ -based MTJ.<sup>12</sup>



## ACKNOWLEDGMENTS

The authors are grateful to K. Hono, S. Kasai, and K. Mukaiyama for useful discussions and critical comments. This work was in part supported by Grant-in-Aids for Scientific Research (S) (Grant No. 16H06332) and (B) (Grant No. 16H03852) from the Ministry of Education, Culture, Sports, Science, and Technology, Japan and also by the ImPACT Program of Council for Science, Technology and Innovation, Japan.

## REFERENCES

- <sup>1</sup>S. S. P. Parkin, C. Kaiser, A. Panchula, P. M. Rice, B. Hughes, M. Samant, and S.-H. Yang, *Nat. Mater.* **3**, 862 (2004).
- <sup>2</sup>S. Yuasa, T. Nagahama, A. Fukushima, Y. Suzuki, and K. Ando, *Nat. Mater.* **3**, 868 (2004).
- <sup>3</sup>Y. S. Choi, Y. Nagamine, K. Tsunekawa, H. Maehara, D. D. Djayaprawira, S. Yuasa, and K. Ando, *Appl. Phys. Lett.* **90**, 012505 (2007).
- <sup>4</sup>S. Isogami, M. Tsunoda, K. Komagaki, K. Sunaga, Y. Uehara, M. Sato, T. Miyajima, and M. Takahashi, *Appl. Phys. Lett.* **93**, 192109 (2008).
- <sup>5</sup>H. Maehara, K. Nishimura, Y. Nagamine, K. Tsunekawa, T. Seki, H. Kubota, A. Fukushima, K. Yakushiji, K. Ando, and S. Yuasa, *Appl. Phys. Express* **4**, 033002 (2011).
- <sup>6</sup>K. Yakushiji, K. Saito, S. Mitani, K. Takanashi, Y. K. Takahashi, and K. Hono, *Appl. Phys. Lett.* **88**, 222504 (2006).
- <sup>7</sup>K. Nikolaev, P. Anderson, P. Kolbo, D. Dimitroc, S. Xue, X. Peng, T. Pokhil, H. Chho, and Y. Chen, *J. Appl. Phys.* **103**, 07F533 (2008).
- <sup>8</sup>T. Furubayashi, K. Kodama, H. Sukegawa, Y. K. Takahashi, K. Inomata, and K. Hono, *Appl. Phys. Lett.* **93**, 122507 (2008).
- <sup>9</sup>J. Sato, M. Oogane, H. Naganuma, and Y. Ando, *Appl. Phys. Express* **4**, 113005 (2011).
- <sup>10</sup>S. Li, Y. K. Takahashi, T. Furubayashi, and K. Hono, *Appl. Phys. Lett.* **103**, 042405 (2013).
- <sup>11</sup>J. W. Jung, Y. Sakuraba, T. T. Sasaki, Y. Miura, and K. Hono, *Appl. Phys. Lett.* **108**, 102408 (2016).
- <sup>12</sup>S. Kasai, Y. K. Takahashi, P.-H. Cheng, Ikhtiar, T. Ohkubo, K. Kondou, Y. Otani, S.

- Mitani, and K. Hono, Appl. Phys. Lett. **109**, 032409 (2016).
- <sup>13</sup>J. M. MacLaren, X. G. Zhang, W. H. Butler, and X. Wang, Phys. Rev. B **59**, 5470 (1999)
- <sup>14</sup>G. Autès, J. Mathon, and A. Umerski, Phys. Rev. B **82**, 115212 (2010).
- <sup>15</sup>S. Kreuzer, J. Moser, W. Wegscheider, and D. Weiss, Appl. Phys. Lett. **80**, 4582 (2002).
- <sup>16</sup>J. Moser, M. Zenger, C. Gerl, D. Schuh, R. Meier, P. Chen, G. Bayreuther, W. Wegscheider, D. Weiss, C.-H. Lai, R.-T. Huang, M. Kosuth, and H. Ebert, Appl. Phys. Lett. **89**, 162106 (2006).
- <sup>17</sup>J. Parkes, R. D. Tomlinson, and M. J. Hampshire, J. Appl. Cryst. **6**, 414 (1973).
- <sup>18</sup>H. W. Spiess, U. Haeberlen, G. Brandt, A. Räuber, and J. Schneider, Phys. Status Solidi B **62**, 183 (1974).
- <sup>19</sup>G. Kresse and J. Furthmüller, Phys. Rev. B **54**, 11169 (1996).
- <sup>20</sup>G. Kresse and D. Joubert, Phys. Rev. B **59**, 1758 (1999).
- <sup>21</sup>S. Baroni, A. Dal Corso, S. de Gironcoli, and P. Giannozzi, [<http://www.pwscf.org>].
- <sup>22</sup>V. I. Anisimov, J. Zaanen, and O. K. Andersen, Phys. Rev. B **44**, 943 (1991).
- <sup>23</sup>G. Sclauzero and A. Dal Corso, Phys. Rev. B **87**, 085108 (2013).
- <sup>24</sup>H. J. Choi and J. Ihm, Phys. Rev. B **59**, 2267 (1999).
- <sup>25</sup>A. Smogunov, A. Dal Corso, and E. Tosatti, Phys. Rev. B **70**, 045417 (2004).
- <sup>26</sup>W. H. Butler, X.-G. Zhang, T. C. Schulthess, and J. M. MacLaren, Phys. Rev. B **63**, 054416 (2001).
- <sup>27</sup>Y. Miura, S. Muramoto, K. Abe, and M. Shirai, Phys. Rev. B **86**, 024426 (2012).